From Transporter to Motor: Evolutionary and Structural Insights into the Emergence of Prestin's Area-Motor Activity in Mammals

Nicolas Fuentes-Ugarte*

Departamento de Biologia, Facultad de Ciencias, Universidad de Chile, Santiago,Chile.

Tiaren Ruiz-Rojas*

Facultad de Ingenieria, Universidad San Sebastian, Santiago, Chile.

Alvaro Ruiz-Fernandez

Computational Biology Lab, Centro Cientifico y Tecnologico de Excelencia, Fundacion Ciencia & Vida, Santiago, Chile, Santiago, Chile.

Jose Antonio Garate

Facultad de Ingenieria, Universidad San Sebastian, Santiago, Chile

Victor Castro-Fernandez†

Departamento de Biologia, Facultad de Ciencias, Universidad de Chile, Santiago, Chile.

Raul Araya-Secchi‡

Facultad de Ingenieria, Universidad San Sebastian, Santiago, Chile and Centro Cientifico y Tecnologico de Excelencia, Fundacion Ciencia & Vida, Santiago, Chile

Abstract

Prestin, a member of the SLC26A family, is essential for the electromotility of mammalian outer hair cells, converting voltage changes into mechanical work. In contrast, non-mammalian orthologues function as anion transporters, lacking electromechanical activity. To investigate the molecular and structural basis of this functional divergence, we performed ancestral sequence reconstruction (ASR) of prestin across vertebrates, followed by comparative structural modeling using AlphaFold2-multimer. We identified more than 200 amino acid substitutions along the lineage that lead to placental mammals, with early substitutions concentrated in the transmembrane domain (TMD) and late substitutions clustering in the STAS domain, particularly in the intervening sequence (IVS). Structural modeling revealed that early substitutions modulate protein–lipid interactions and interhelical contacts. In placental mammals, the IVS-loop adopts a distinct conformation that places a negatively charged patch near the chloride access pathway, potentially affecting the ion dynamics and voltage responsiveness. These structural transitions occurred without major rearrangements of the global fold of prestin, supporting a notion in which the novel function evolved through distributed substitutions within a conserved scaffold. Our findings illustrate how molecular exaptation, and incremental structural remodeling enabled the repurposing of an ancestral anion transporter into a voltage-sensitive area-motor, providing a framework for understanding the molecular evolution of complex biophysical traits central to auditory neuroscience.

KEYWORDS

prestin evolution, ancestral sequence reconstruction, SLC26A family, electromotility, voltage-sensitive membrane proteins, STAS domain, IVS-loop.

INTRODUCTION

The auditory system of mammals exhibits remarkable sensitivity and frequency selectivity. These features rely on the cochlear amplifier, a mechanism that enhances sound-induced vibrations within the cochlea to improve sensitivity and frequency resolution. At the heart of

* These authors contributed equally to this work

† Corresponding author: vcasfe@uchile.cl

‡ Corresponding author: raul.araya@uss.cl

this amplification process are outer hair cells (OHCs), specialized sensory cells that exhibit electromotility (EM), the ability to rapidly change body length in response to electrical stimulation[1, 2, 3, 4, 5]. EM is driven by the area-motor protein prestin, densely packed in the lateral membrane of OHCs[3, 6, 7].

Prestin is a member of the SLC26A family, which predominantly comprises anion transporters[8]. As such, non-mammalian prestin orthologs function as non-electrogenic anion exchangers[9, 10, 11], while mammalian prestin has evolved into a direct voltage-to-displacement converter, operating on millisecond or faster timescales, which are essential for high-frequency sound amplification[3, 5, 7, 12, 13].

Phylogenetic analyzes have revealed that mammalian prestin evolved from an anion transporter present in a pre-mammalian ancestor[14, 15, 16]. Mammalian prestin exhibits minimal transport capacity and pronounced nonlinear capacitance (NLC), a hallmark of voltage sensitivity[11, 17, 18]. Furthermore, an inverse relationship has been established between anion transport and motor function, suggesting that transport capacity was lost as voltage-dependent NLC was gained [10, 19]. Thus, the unique function of mammalian prestin is the result of evolutionary adaptations that have repurposed an ancestral anion transporter into a highly specialized motor protein. This functional shift from ion transport to electromotility remains incompletely understood, particularly with regard to how key substitutions have fine-tuned this mechanism in placental mammals.

Considerable efforts have been devoted to identify the regions and residues where the differences between mammalian and non-mammalian prestin are most pronounced and critical for the generation of NLC and EM. Early work identified specific segments within the transmembrane domain (TMD), notably TM1–2 and TM9–11, as essential to NLC/EM and determined that replacing these regions in the zefrafish prestin by those of gerbil, a synthetic prestin capable of transport and NLC could be constructed[20]. Others showed that the extracellular loop between TM3 and TM4 (EC-loop) is also essential for NLC/EM[21, 22, 23]. Furthermore, increased flexibility of TM6 was proposed to contribute to NLC/EM[24], as well as certain conserved and non-conserved cysteines[25]. In addition, membrane thickness has been shown to affect mammalian and non-mammalian prestin differently[26].

Recently, the structures of human(HsPres)[27], dolphin(TtPres)[24], and gerbil (MuPres)[28] prestin have provided invaluable information on its functional organization and its interac-

tions with the lipid membrane. From these structures, molecular dynamics (MD) simulation studies have shown the existence of elevator-like movements as part of its conformational change cycle[29] and how prestin structure affects the organization of the membrane in its surroundings[30]. However, fundamental questions remain regarding the identity of the voltage sensor (extrinsic or intrinsic)[9, 31, 32], how voltage triggers conformational change[24, 33, 34], and how disordered regions, absent in experimental structures such as the IVS-loop, contribute to the specialized function of mammalian prestin[35].

Here, we address these gaps employing ancestral sequence reconstruction (ASR) combined with structural modeling and conformational sampling to identify and contextualize key substitutions in prestin evolution. We map these changes to prestin domains and regions and then use conformational sampling with AlphaFold2-multimer (AF2-multimer)[36, 37] to evaluate their structural effects. This approach not only corroborates the relevance of known functional sites, but unveils previously unexplored features, notably in the IVS-loop of the STAS domain. By modeling non-mammalian prestin structures for the first time, we offer an evolutionary perspective on how incremental substitutions collectively reshaped an ancestral anionic transporter into the high-speed area-motor protein essential for mammalian hearing.

Our results indicate that early substitutions alter contacts between residues on the TMD and between the protein and the surrounding lipids, which point toward a gradual reduction in transport capacity along with an enhanced voltage sensitivity. Despite these functional changes, the TMD architecture remains largely unchanged until more punctuated substitutions appear after the divergence between mammals and reptiles. These later substitutions cluster in the EC-loop and, more strikingly, in the IVS of the STAS domain, giving rise to pronounced structural differences between non-mammalian and mammalian prestin. In particular, alterations in the IVS-loop result in the emergence, in placental mammals, of a patch of negatively charged residues (negative patch or NP) that could influence the access/exit of chloride ions from the binding site, suggesting a pivotal role for this region in the unique electromechanical behavior of mammalian prestin.

RESULTS AND DISCUSSION

Ancestral Sequence Reconstruction Identifies Critical Evolutionary Substitutions in Prestin Domains.

We constructed a phylogenetic tree for the chordate SLC26A5 subfamily as shown in Figure 1 A (for a full version of the tree, see Supplementary File 1), identifying five monophyletic groups (fish, amphibians, reptiles, birds and mammals) with a consistent topology compared to previous studies [38, 39]. Using ancestral sequence reconstruction (ASR)[40], we inferred 12 ancestral sequences, listed in Table I, with high confidence (mean posterior probability > 0.95; see also Supplementary Figures S1, S2 and S3).

Our analysis focused on the evolutionary pathway from fish to placental mammalians (ancPis $\rightarrow$ ancRhi $\rightarrow$ ancTre $\rightarrow$ ancAmn $\rightarrow$ ancMam $\rightarrow$ ancThe $\rightarrow$ ancPla; following the nomenclature introduced in I) using as initial reference (outgroup) the closest homologous transporter, human SLC26A6 (hsA6), and human SLC26A5 (hsPres) as a model of current placental mammalian prestin. Sequence identity was high within groups (90% in non-mammals, 80% in mammals), and dropped to 60% between them (Supplementary Table S1).

We identified 207 substitutions along this evolutionary pathway: 42 in the N-terminal domain, 83 in the transmembrane domain (TMD) and 82 in the sulfate transporter and anti-sigma (STAS) domain. Substitutions were classified as early (ancAmn $\rightarrow$ ancMam; n=108), intermediate (ancMam $\rightarrow$ ancThe; n=19), or late (ancThe $\rightarrow$ ancPla; n=21), plus four earlier substitutions (ancTre $\rightarrow$ ancAmn). We also found substitutions showing two (n = 38) and three steps (n=17) in the transition from ancAmn to ancPla (or hsPres) that are indicative of regions with greater variability (the complete list of substitutions is presented in the Supplementary Tables S2, S3, S4, S5 and in the Supplementary File 2). In terms of proportions, *i.e.* the percentage of substituted residues, the N-terminal domain presents a 56% of substitutions, the TMD 19% and the STAS domain 35%, suggesting that the TMD is more conserved and less prone to substitutions.

Regarding the nature of the substitutions, we found that 47% (n = 97) of the substitutions are non-conservative, i.e., they significantly change the chemical properties of the residue (indicated in **bold*** throughout the text). They correspond to 31% of the substitutions

Table I. Robustness of the Ancestral Sequence Reconstructions.

Ancestor	Description	Node Support	ASR Mean Posterior probability ± SD
ancPis	Last common ancestor from Pisces	99.98%	0.974 ± 0.092
ancRhi	Last common ancestor from Rhipidistia	96.68%	0.972 ± 0.095
ancTre	Last common ancestor from Tetrapoda	99.98%	0.952 ± 0.125
ancAmp	Last common ancestor from Amphibia	77.94%	0.973 ± 0.090
ancAmn	Last common ancestor from Amniota	99.98%	0.974 ± 0.088
ancRep	Last common ancestor from Reptilia	93.41%	0.977 ± 0.083
ancArch	Last common ancestor from Archosauria	99.98%	0.978 ± 0.081
ancAvi	Last common ancestor from Avis	99.98%	0.976 ± 0.084
ancMam	Last common ancestor from Mammalia	99.98%	0.959 ± 0.108
ancThe	Last common ancestor from Theria	99.98%	0.962 ± 0.113
ancMar	Last common ancestor from Marsupialia	99.98%	0.996 ± 0.033
ancPla	Last common ancestor from Placentaria	99.98%	0.999 ± 0.001

in the N-terminal domain, 45% in the TMD, and 52% in the STAS domain. According to our findings, these substitutions tend to correspond to late, 2-step, or 3-step substitutions. Interestingly, the most prevalent types of non-conservative substitutions were those that result in the addition of glycines or prolines and those that result in the replacement of an apolar for an aromatic sidechain.

In summary, our reconstruction reveals that prestin evolution involved a substantial number of amino acid substitutions, with a strong bias toward late, non-conservative changes in the STAS domain and to a lesser extent in the TMD. The prevalence of substitutions that add glycine or proline, and apolar-to-aromatic substitutions highlights potentially function-altering events that occurred during the transition from ancestral transporters to the specialized motor protein observed in placental mammals.

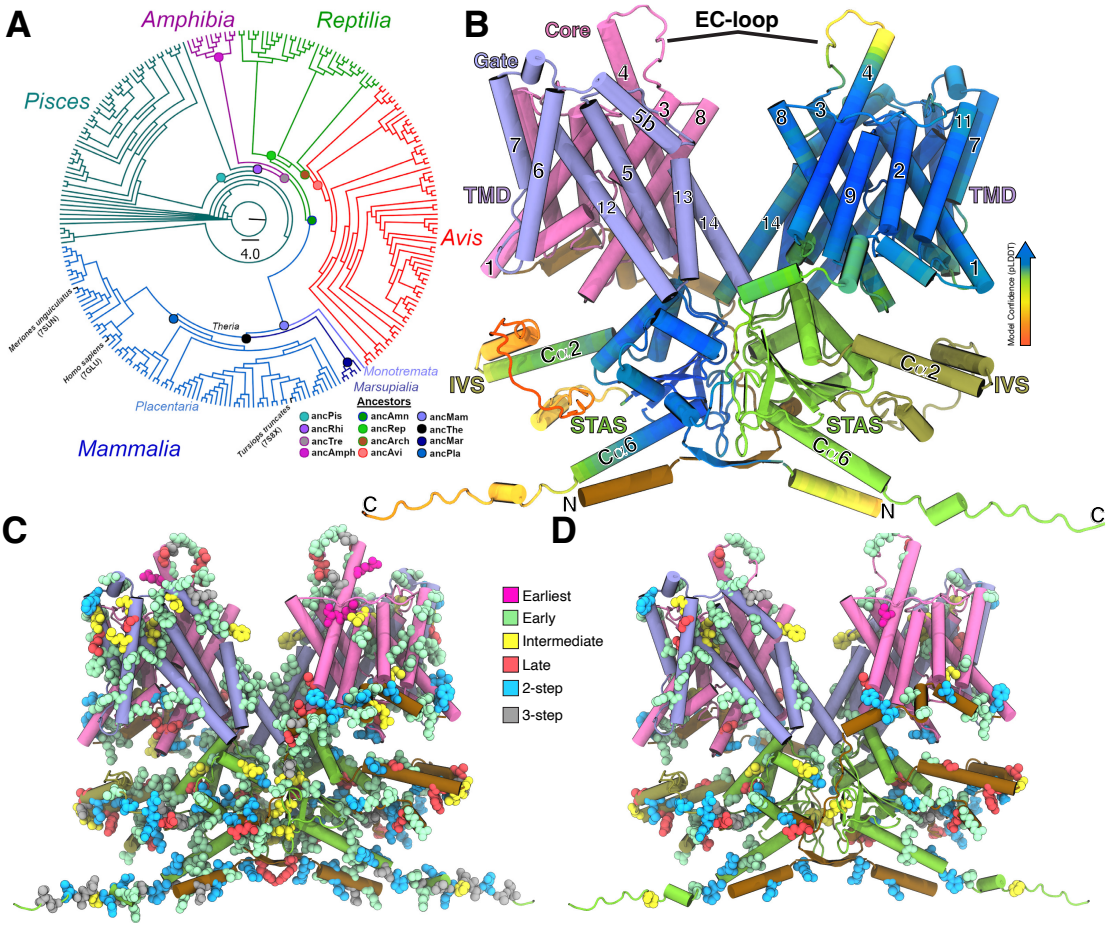

Figure 1. **Ancestral sequence reconstruction of SLC26A5 members**(A) Maximum likelihood phylogenetic tree of prestin (SLC26A5) from Chordata. Sequences colored as follow: Dark cyan Pisces, dark magenta Amphibian, green Reptilian, red Birds, light blue monotremata mammalians, navy blue marsupialia mammalians and bright navy blue placentaria mammalians. The extant sequences of *Homo sapiens (hsPres)*, *Meriones unguiculatus (muPres)* and *Tursiops truncates (ttPres)* are highlighted with their respective PDB accession codes. Circles indicate nodes where ancestral sequences were inferred in this study. (B) Structural model of full-lenght hsPres. Protein shown in cartoon representation with the monomer on the right labeled by AF2 confidence score (pLDDT) and the other by domain (N-terminal domain, ochre; core domain, pink; gate domain, violet: STAS domain, light-green and IVS, tan. (C-D) Mapping of the substitutions onto the hsPres model showing (C) all and (D) non-conservative substitutions. Domains colored as in B and substitutions colored as: earliest, magenta; early, lime; intermediate, light-yellow; late, red; 2-step light-blue; and 3-step, gray.

Conformational Sampling Reveals that the IVS-loop of the STAS domain differentiates mammalian Prestin.

Placing the substitutions in the context of prestin structure is crucial to understanding their functional relevance. Thus, we generated a full-length model of human prestin (hsPres) using AlphaFold2-multimer (AF2-multimer) (V3)[36, 37] to account for the regions missing in the available mammalian prestin structures, particularly the IVS-loop. In addition, we generated structural models for ancestral and extant prestin representatives (Figure 2 and Supplementary Figure S4). The models closely resembled the domain-swapped dimeric structure of members of the SLC26A family (Figure 1 B) and showed high overall confidence, indicated by the high values of the predicted local distance difference test (pLDDT) observed for most of the well-folded part of the TMD and STAS domain (Figure 1 B, Figure S4 and Supplementary Figure S4). The flexible and disordered parts (N- and C-terminal, EC-loop, IVS-loop) show the lowest pLDTT values, indicating low confidence.

Since structural predictions of flexible regions such as the EC-loop and the IVS-loop show low confidence, the use of structural ensembles provides a broader scope of their functional relevance. Thus, we generated structural predictions of hsPres, prestin ancestors (ancAmn, ancRep, ancThe, ancMam, ancPla) and chicken prestin (chkPres) increasing their conformational variability by using multiple seeds and the *dropout* option (see Methods) of AF2-multimer(V3) as reported in[41]. This resulted in the generation of 1280 predictions for each sequence that explored the flexibility of the EC- and IVS-loop while showing minor variation in the TMD and folded parts of the STAS domain. However, it is important to note that, while this approach enhances conformational sampling, the resulting ensembles have to be interpreted as a qualitative exploration of possible conformations rather than a quantitative representation of a thermodynamic ensemble of populations.

Across all reconstructed prestin models, the transmembrane domain (TMD) exhibited high structural similarity (RMSD-C$\alpha \leq 3.0$ Å), with variation in the TM3-M4 loop (extracelular or EC-loop) and the TM6-TM7 loops. Similarly, for the structured part of the STAS domain. Strikingly, the only major structural divergence observed between non-mammalian and mammalian models (ancestral and extant) was in the conformation and orientation of the intervening sequence (IVS) loop.

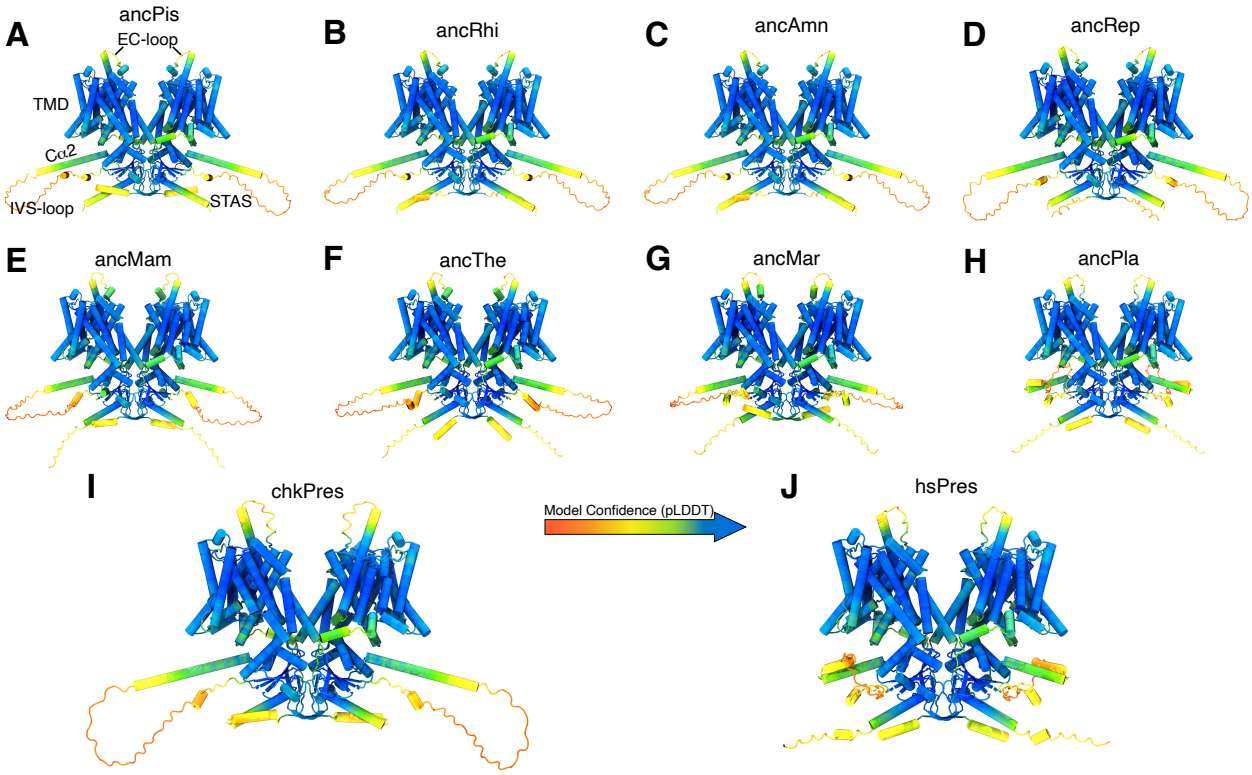

Figure 2. **Reconstruction of ancestral prestin structures using AF2-multimer(V3).** Structural predictions of ancestors from Pisces (A), Rhipidistia (B), Amniota (C), Reptilia (D), Mammalia (E), Theria (F), Marsupialia (G), Placentaria (H), chicken prestin (I) and human prestin (J) shown in cartoon representation colored by confidence (pLDDT).

In non-mammalians ancestors and extant representatives, the IVS consistently formed an extended Cα2 helix (Figure 2A-D and Supplementary Figure S4 A-I). In contrast, mammalian ancestors and extant representatives exhibited a distinct rearrangement of this region. Early mammalians and marsupials (ancMam, ancThe, platypus, opposum, wombat) showed a shorter Cα2 helix followed by a disordered IVS-loop (Figure 2 EF and Supplementary Figure S4 JL) while placental mammals (ancPla, human, gerbil, dolphin, and bat) showed a broken helix (Cα2 + Cα2') repositioning the IVS loop toward the intracellular entrance of the adjacent monomer (Figure 2 GH and Supplementary Figure S4 MH).

This consistent difference in conformation and orientation of the IVS-loop is correlated with the differences observed between sequences of non-mammalian and mammalian ancestors and between early mammalians, marsupials and placentals (Supplementary Figure S3 and Supplementary File 2). Furthermore, they are in line with the progression of prestin function

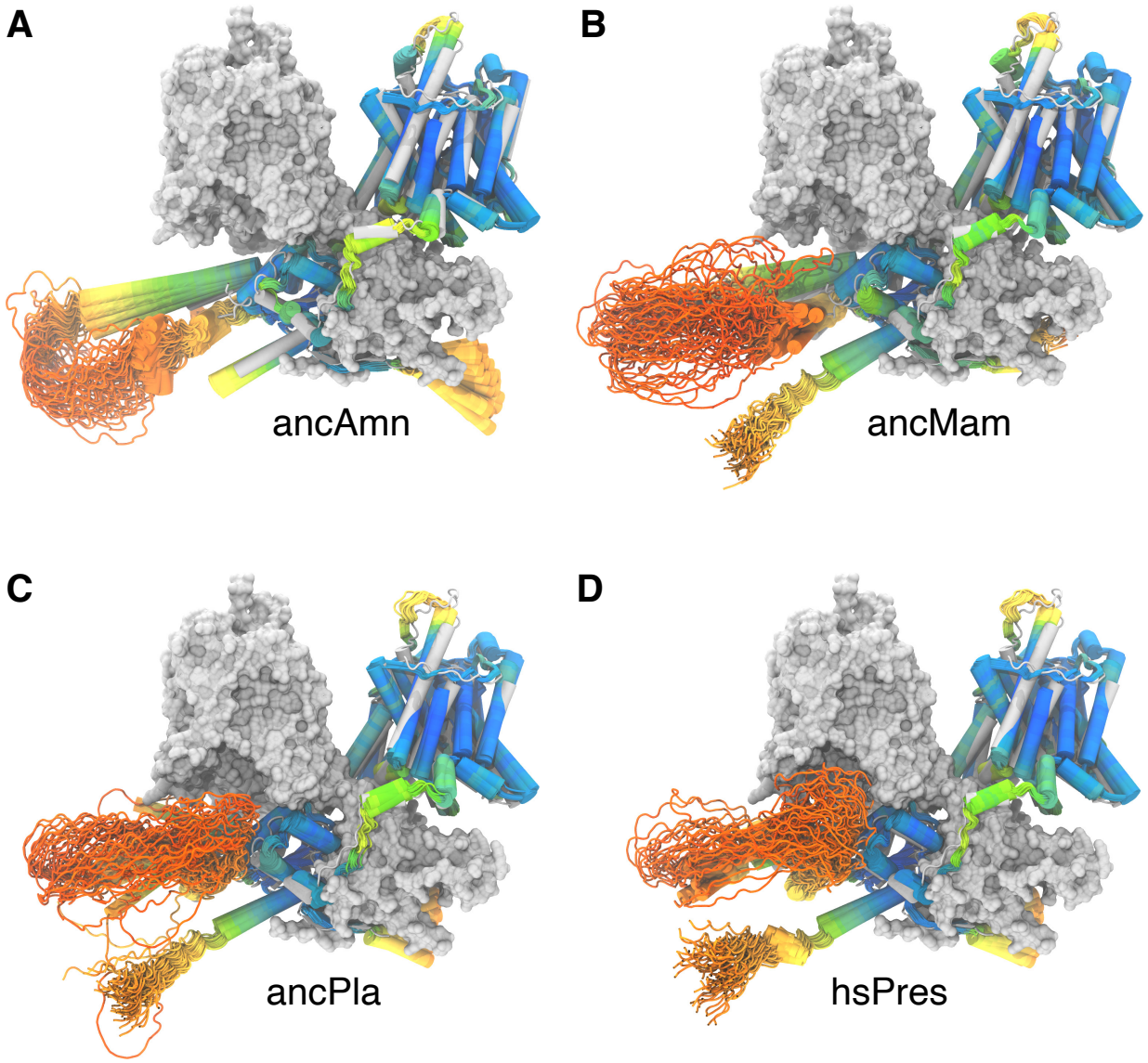

Figure 3. **Conformational sampling of prestin models**(A-D) Representative conformations obtained for human and ancestral prestin models. Only one monomer of the models is shown in cartoon representation colored as in Figure 2. The other monomer corresponds to hsPres structure 7LGU[27] shown as a gray surface.

from ion transport in non-mammals followed by intermediate area-motor adaptations in monotremes to robust, finely tuned electromotility in therian mammals[16, 42, 43]. Thus, the IVS-loop represents the most prominent structural difference distinguishing mammalian prestin from their ancestral and non-mammalian counterparts. We discuss the relationship between these differences and the substitutions that we found in that region in a later section of this work.

Mapping of substitutions into the structural models of hsPres and the reconstructed ancestors.

Mapping the substitutions on the hsPres model (Figures 1 CD and 4), we observed that the early substitutions are distributed throughout the TMD and STAS domains with non-conservative early substitutions accumulating in the TM5b, TM6, EC-loop and STAS domains (Figure 1 D, 4). Intermediate substitutions are found mainly in TM5b, TM6 and in the STAS domain. Late substitutions are found in the EC-loop, the TM5b-TM6 loop, and in the STAS domain. Finally, two- and three-step substitutions are found in the EC-loop and STAS domains, indicating positions with the least restriction to substitutions. In the following sections, we detail our analysis for each domain separately.

Substitutions to the TMD show clustering in the Gate Domain.

Almost 20% of the residues in the TMD (n=83) are substituted during the ancAmn →→ ancPla transition, with 9% corresponding to non-conservative substitutions. In our analysis, we found that the early and intermediate substitutions are located near and far from the chloride-binding site, whereas the late substitutions are positioned farther away from it. (Figure 1 CD and Figure 4). This suggests that early and intermediate changes, which are widespread across the transmembrane domain (TMD) and do not necessarily affect chloride binding, may have contributed to the loss of ion transport and the emergence of voltage sensitivity. However, late substitutions, mapped to a few clustered locations, may be responsible for the fine-tuning of prestin to provide the high sensitivity and selectivity observed in placental mammals[16].

Not all TM helices are equally substituted, and we found more substitutions in the gate domain (scaffold) than in the core domain (transport) with the highest number of substitutions found in TM5b, TM6 and TM12 (Figure4, II and Supplementary FigureS3). Furthermore, in both domains the majority of substitutions are located in the external face of the helix, with the exception of TM6 and TM7. In these helices, their lipid-facing region, which also forms the interface between the two, concentrates all the substitutions (Figure 4 BD).

It has been shown that the function of prestin and other members of SLC26A involves changes in the orientation between the core and gate domains [24, 27], thus, we expected

Table II. Summary of TM Helices Substitutions

TM Helix	Substitutions	NC Substitutions	Evolutionary Step
TM1	8/29	5	2-step, early and intermediate
TM2	2/17	2	1 early, 1 intermediate
TM3	3/14	2	All early
TM4	5/27	4	3 earliest, 1 late, 1 3-step
TM5	2/23	2	Early
TM5b	7/11	4	4 Early, 2 intermediate, 1 3-step
TM6	11/23	10	7 Early, 2 intermediate, 2 late
TM7	9/15	6	6 early, 1 intermediate, 1 late, 1 2-step
TM8	4/35	4	1 early, 2 late, 1 2-step
TM9	2/17	1	1 early, 1 intermediate
TM10	2/9	2	1 early, 1 2-step
TM11	7/21	3	all early
TM12	5/27	5	4 early, 1 intermediate
TM13	4/15	4	all early
TM14	4/20	2	all early

to find an accumulation of substitutions in their interface. However, as can be seen in Figure 4 AB, very few substitutions are found at the core-gate interface. From the core domain, we found M93L (TM1), Y101F (TM1), M353V (TM8) and MI397L (TM10) and from the Gate domain, we found only Q225M* (TM5). Some of these substitutions are located near the chloride binding site, which highlights their relevance for NLC/EM. For example, in TM1 substitutions M93L and Y101F (early) and **T136P*** (intermediate) when mutated individually from their mammalian to non-mammalian version (that is, L93M, F101Y, P136T) resulted in changes in the parameters of NLC and when mutated together completely abolished NLC/EM [20]. Furthermore, mutated V353 and L139 were related to changes in solvent accessibility to the chloride binding site[29].

Despite the lack of substitution on the core-gate interface, we found a network of substitutions located near the linkers between both domains between TM7-TM8 and TM11-TM12. These include a combination of early, intermediate, and late substitutions located on the extracellular side of TM5, TM5b, TM6, TM7, and TM12 in the gate domain and the extracellular side of TM11 in the core domain (Figure 4) and may have changed the coupling between domains and therefore the functional conformational change.

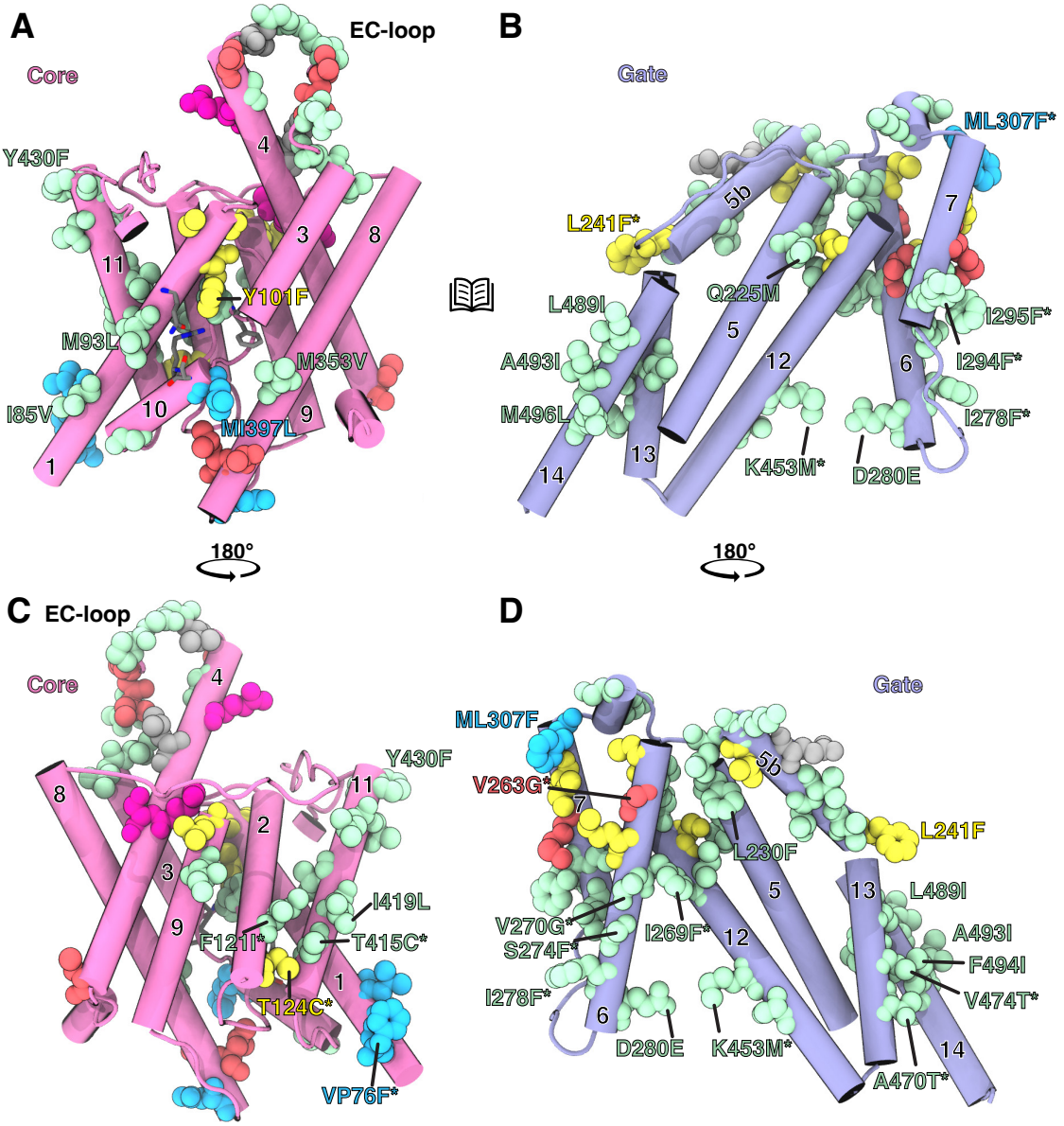

Figure 4. **Substitutions on the TMD**(A-B) Open-book view of the core (A) and gate (B) domain interface. (C-D) 180° rotation along the z-axis of the core domain (C) and gate domain (D) with respect to A and B respectively. In all panels the protein is shown in cartoon representation and substituted residues in VdW representation. The same color scheme as in Figure 1 BD was used. Two-step substitutions are represented as, for example, VP76F, with residue numbering based on human prestin (HsPres).

One of the helices in the TMD with the largest amount of substitutions is TM6, with the majority being non-conservative. This helix has been suggested to play a crucial role in NLC/EM due to the accumulation of glycines, in a unique pattern in mammalian prestin[24]. Our analysis showed that of the glycines found in placental prestin, two correspond to early substitutions and one to a late substitution (Figure 5 D). Furthermore, we found several substitutions in TM6 that could also be relevant for its flexibility since they participate in interactions with TM7 and TM12 (Figure 4 BD and Figure 5) and could restrict rotation or displacement of TM6. Furthermore, a comparison with the non-mammalian ancestor ancAmn shows that early substitutions D280E in TM6, and **K543M*** in TM12 perturb an electrostatic contact network between these helices (Figure 5), which would reduce the strength of the interaction between them and allow TM6 to move more freely. Other charged residues that are part of this network, in mammalian prestin, have been shown to affect NLC/EM when mutated to glutamine[32], highlighting the role of the interaction of TM6 - TM12 in prestin function.

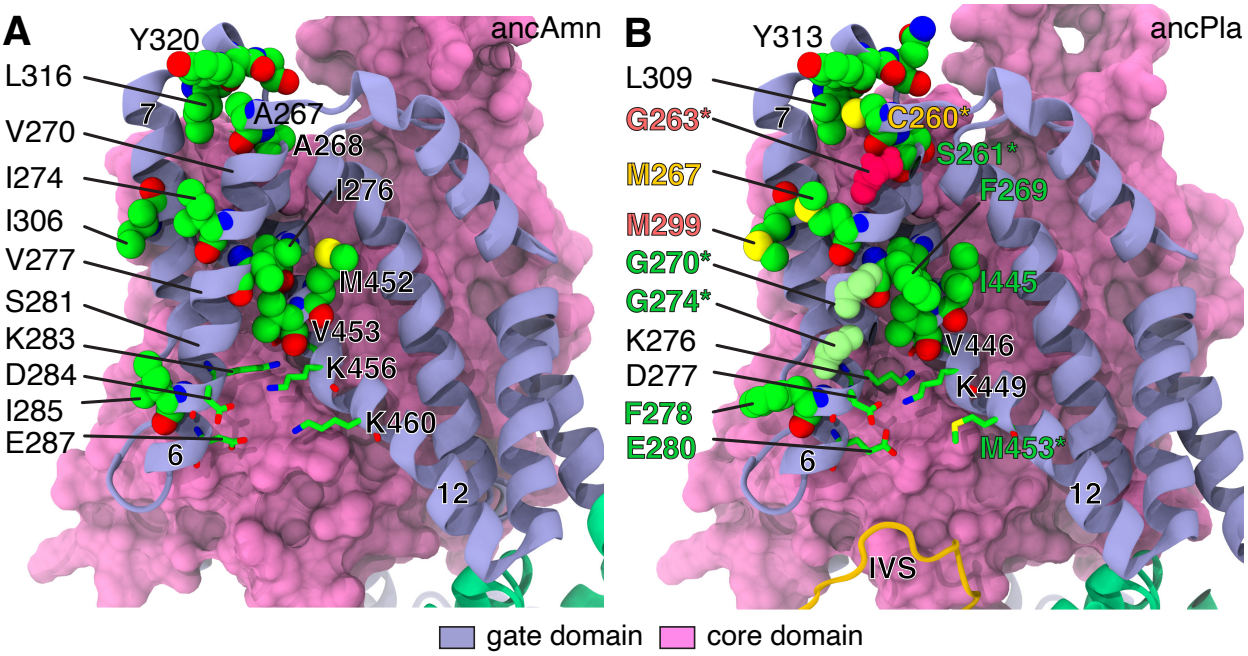

Figure 5. **Substitutions in the TMD**. (A-B) Substitutions in TM6 in the ancAmn (A) and ancPla (B) models. The gate domain is shown as ribbons and the core domain as surface colored as in 1. Substitution labels are colored as in 1C and shown in VdW or licorice representation colored by element (carbon, green; oxygen, red; nitrogen, blue and sulphur, yellow). Only the TMD of one monomer is shown for clarity. Non-conservative substitutions marked with a *.

Several Substitutions in the TMD affect protein-lipid interfase.

Mammalian prestin is known to be sensitive to changes in membrane tension[44, 45, 46], thickness [26, 47, 48], and cholesterol concentration[49, 50, 51] thus it called our attention that most of the substitutions found in the TMD are located on the lipid-facing side of the helices, particularly in the gate domain (Figure 4). This suggests that the evolutionary transition from transporter to area-motor may have involved significant changes in how prestin interacts with the membrane. Interestingly, previous studies have identified differences in the response to changes in membrane thickness between mammalian and non-mammalian prestin [26, 48], providing some support for our observations.

We identified two sets of non-conservative substitutions that may be the most relevant: The first set comprises eight substitutions in which an apolar residue is replaced by phenylalanine (and one where a tyrosine is replaced by a phenylalanine). They are mainly located near the extracellular or intracellular end of an helix and concentrate in the gate domain (TM5b, TM6 and TM7) with only two found in the core domain (TM1 and TM11) (4). The second set of substitutions comprised four early non-conservative substitutions in TM13 that result in a unique pattern found only in mammalian prestin (**V470T***, **V474T***, **A475T*** and **A478S***). In our mammalian models, residues V474, S478, and T479 (residue numbering according to hsPres) are located on the external face of the helix, while T475 faces inward toward TM5. This results in three polar residues placed inside the lipid bilayer in the intermonomer region (Figure6). These residues could use their side chain hydroxyl groups to form intrahelix (TM13) and interhelix (TM13-TM14) hydrogen bonds, a characteristic that has previously been observed when these types of residue are located in transmembrane helices [52]. Furthermore, the presence of polar residues such as Ser or Thr in the lipid bilayer has been shown to affect the thickness of the membrane and the organization of lipids around the protein [52]. More importantly, these residues increase the polarity in the intermonomer region, facilitating the interaction with the poplar head-groups of lipids or cholesterol.

In summary, we found several substitutions (mostly early) that suggest that one of the initial changes in mammalian prestin is related to its interaction with surrounding lipids. It is well known that substitutions in transmembrane helices that replace an apolar residue with a phenylalanine or a threonine can affect the disposition of the TM helix or result in

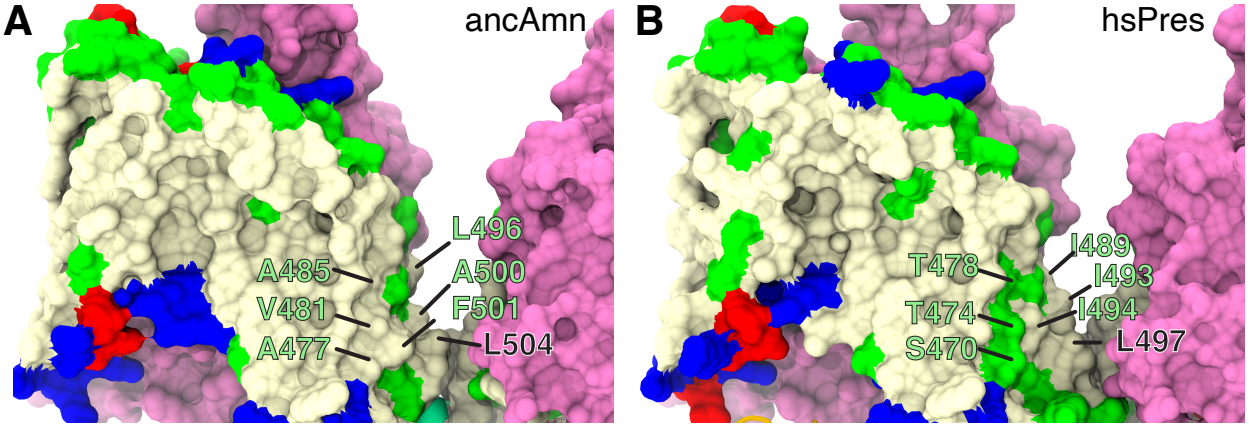

Figure 6. **Substitutions on the TM13-14**(A-B) (A-B) Surface representation with the core domain colored as in Figure 1B and the gate domain colored by residue type (hydrophobic = white, polar = green, acidic = red, basic = blue). (A) ancAmn (B) ancPla. The same color scheme as in Figure 1 (C) was used to label the substitutions.

remodeling of protein-lipid interactions, membrane embedding and orientation, and helix-helix interactions and dynamics[53, 54, 55]. Furthermore, these changes not only alter the protein itself but also cause the surrounding lipid and protein environment to adapt, affecting protein stability, conformational equilibrium, and interactions. Thus, these substitutions could be associated with the membrane deformation around human prestin and its lipid-mediated organization[27, 30] and the differences in response between mammalian and non-mamalian prestin to changes in membrane thickness[26].

EC-loop configurations correlate with functional differences between non-mammalian and mammalian prestin.

In the TMD we also find the extracellular loop (EC-loop), which joins TM3 and TM4 (residues 151 to 170 in hsPres). It has been shown to provide pendrin (SLC26A4) with NLC / EM when its EC-loop is replaced by that of gerbil prestin[21], while other studies have proposed that it plays a key role in EM[22, 23]. We map five early, three late, and one 3-step substitutions in this region, a remarkable accumulation for a 20 residue loop (Figure 7A). As expected, substitutions resulting in a PGG motif produce a different conformation and orientation of the loop between non-mammalian and mammalian ancestors (Figure 7). In non-mammalian ancestors, the loop faces the extracellular surface of its monomer,

facilitating the formation of interactions with residues from TM4, the TM5-TM5b loop, and TM5b. In mammalian ancestors, the loop points outwards, decoupling TM3 and the loop from other regions, a situation that is more marked for the placental ancestor ancPla and hsPres.

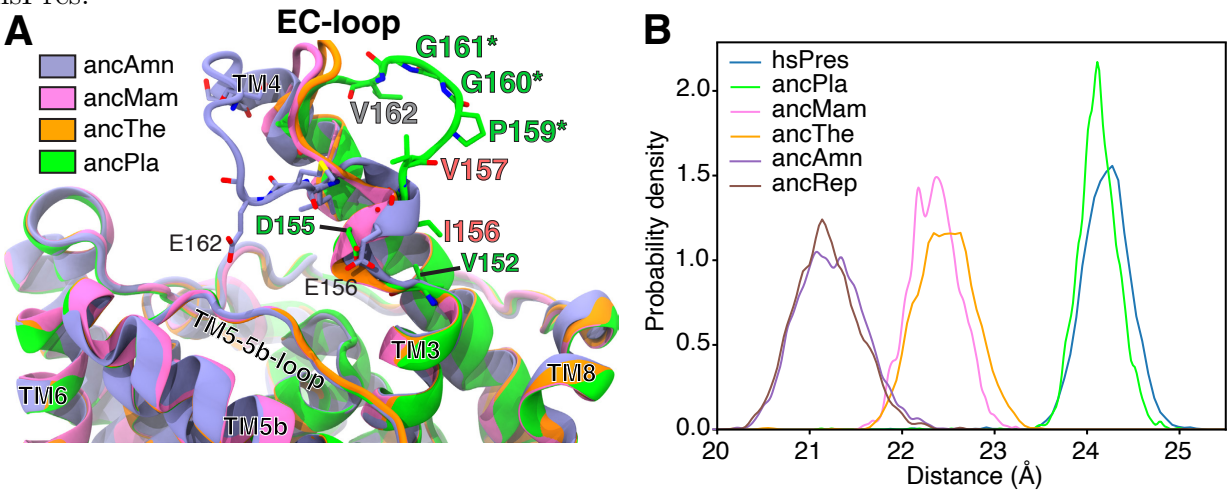

Figure 7. **Structural effect of substitutions in the EC-loop**. (A) Substitutions in the EC-loop. Proteins shown as ribbons. Substitution labels colored as in Figure 1B. Non-conservative substitutions marked with a *. (B) Distribution of the distance between the Center of Mass (COM) of the EC-loop and the COM TM5b obtained from the models AF2-conformational sampling models

Conformational sampling further highlights these differences, as shown by the distinct distance distributions between the center of mass (COM) of the EC-loop and the COM of TM5b obtained from the models sampled in Figure 7 B): non-mammalians (ancAmn, ancRep, average distance $\sim$ 21 Å), early mammalians (ancMam, ancThe, average distance $\sim$ 22 Å) and placentals (ancPla, hsPres, $\sim$ 24 Å).

Taken together, our results suggest that substitutions in the EC-loop alter its conformational flexibility and its capacity to interact with other regions of the TMD, particularly by decoupling it from the TM5-5b loop. However, our results do not allow for a mechanistic explanation of the role of the EC-loop on the generation of NLC/EM. Interestingly, TM5b and the TM5-TM5b loop present several early substitutions and its structural/functional role remains unexplored, so it is an interesting area for future research.

A Unique IVS-loop in Placental Mammalian Prestin results from accumulation of substitutions

In the STAS domain, the greatest accumulation of substitutions is found in the intervening sequence (IVS) that connects Cα1 to sheet Cβ4 (residues 561 to 614 according to hsPres) and contains helix Cα1 (8AB). This segment is highly variable across the SLC26A family, both in length and in amino acid composition[8].

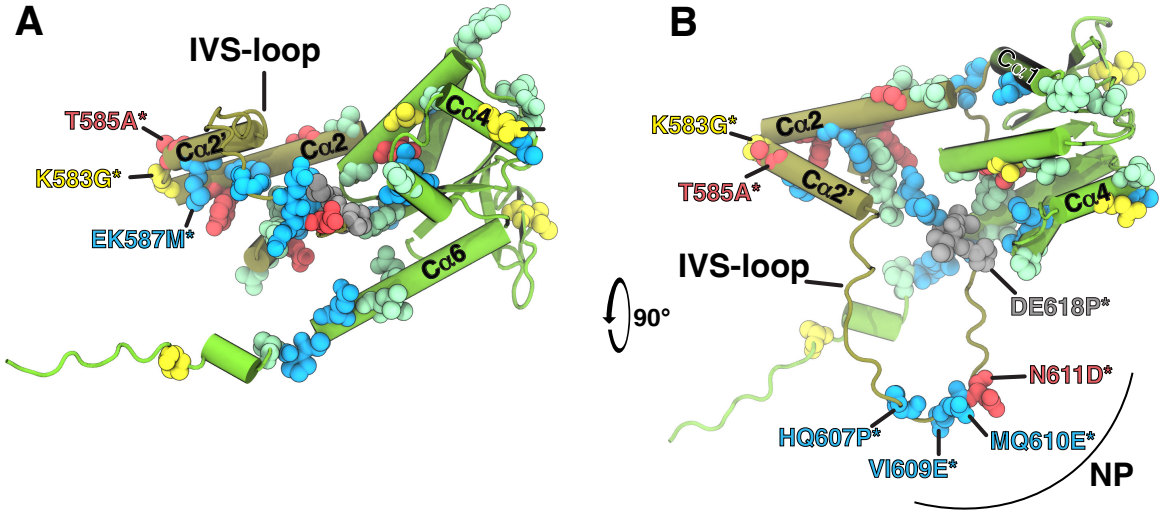

Figure 8. **Substitutions in the IVS** (A-B) Detail of the STAS domain showing only the non-conservative substitutions, highlighting substitutions found in the IVS-loop and the negative patch (NP). (A) Side view and (B) Top view (90° rotation of A along the x-axis). In all panels the protein is shown in cartoon representation and substituted residues in VdW representation. The same color scheme as in Figure 1 (BD) was used.

In the IVS there is a flexible loop (IVS-loop) that connects helix Cα2 with sheet Cβ4 (residues 580 to 614 according to hsPres) that is unresolved in all currently available prestin structures and in most of the members of the SLC26 family. The only exception is a set of SLC26A3 cryo-EM structures (PDB-ID: 7XUH, 7XUJ, 7XUL, and 8IET) in which the IVS loop is resolved and placed near the intracellular entry of the adjacent monomer (FigureS5). Unfortunately, there is no publication associated with these structures.

Despite its variability, it has received limited attention in studies of the function and regulation of prestin and other members of the family. Some reports suggest potential roles in protein-protein interactions with regulators such as calmodulin[56, 57] or CTFR [58, 59].

One study found that mutations in positively and negatively charged residues within the mammalian prestin IVS loop caused modest changes in voltage operating parameters[35]. More recently, the IVS-loop in SLC26A9 has been implicated in modulating intracellular chloride dynamics[60].

In this region, we found 30 substitutions that result in clear sequence differences between non-mammalian, early mammalian and placental ancestors (Figure 9A and Supplementary Figure S3), which include the elimination of a positively charged patch (PP in Figure 9 A) and the appearance of a negatively charged patch in placental mammals (NP in Figure 9A). These differences also translate into structural differences in our models. Mammalian ancestors (ancThe onward) present the non-conservative intermediate substitution **K583G*** which result in a broken Cα2 in two helical segments: Cα2 and Cα2' as observed in the ancPla and hsPres models (Figure 2 (GH and J), 16 BE, Figure 9 B) (and other mammalian representatives; Supplementary Figure S4 MM). This characteristic is more pronounced in the ancPla and hsPres models (see Figure 9 B), perhaps due to substitutions at positions 584 (3-step), 585 (late) and 587 (2-step), resulting in the NANMANA motif that has a higher helix propensity. After Cα2', we find Pro607 (two-step) and, more notably, three two-step substitutions that replace hydrophobic or polar residues with negatively charged amino acids (Glu609, Glu610, and Asp611) (16 BE) increasing the number of negatively charged residues resulting in a negative patch (NP) formed by residues Glu609, Glu610, and Asp611 (Figure 9 A). This combination of substitutions results in the placement of the NP near the entrance of the intracellular (IC) cavity of the adjacent monomer (Figure 9B-D). The NP is adjacent to the PIVKSTF motif, which is unique to placentals and originated from a series of two- and three-step substitutions. This motif forms contacts with residues from helix Cα3 and with a group of substitutions in helix Cα5 (Pro696 (early non-conservative, S to P), Ala697 (two-step, T to S to A), Leu698 (two-step, T to V to L)) that increase the hydrophobicity of this helix (16BE). Thus, changes that lead to the formation of Cα2' and NP are accompanied by changes in other regions of the STAS domain that could stabilize this unique conformation.

Conformational sampling showed that non-mammalian ancestors present a continuous and extended Cα2 positioning of the IVS-loop far from the intracellular (IC) entrance of the adjacent monomer. In contrast, mammalian models, especially those representing placental

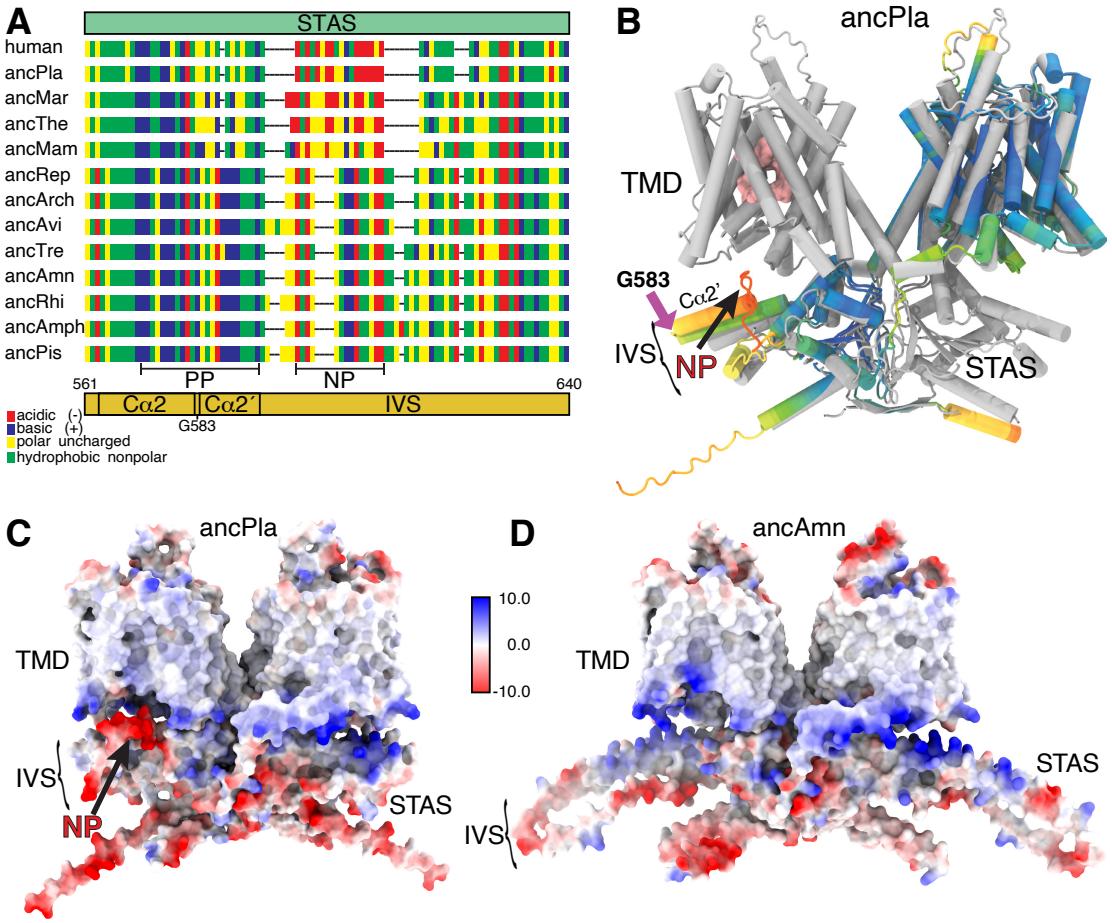

Figure 9. **Detail of the unique features of the placental mammal IVS**. (A) Fingerprint sequence alignment of the reconstructed ancestors and hsPres. Residues colored by hydropathy (acidic, red; basic, blue, polar uncharged, yellow and hydrophobic nonpolar, green). NP and PP refer to negative and positive patch, respectively. (B) Superposition of a monomer of the ancPla model (colored by pLDDT as in Figure 2) onto the structure of human prestin 7LGU [27] (grey) shown in cartoon representation. (C-D) Electrostatic potential maps of ancPla (B) and ancAmn (C).

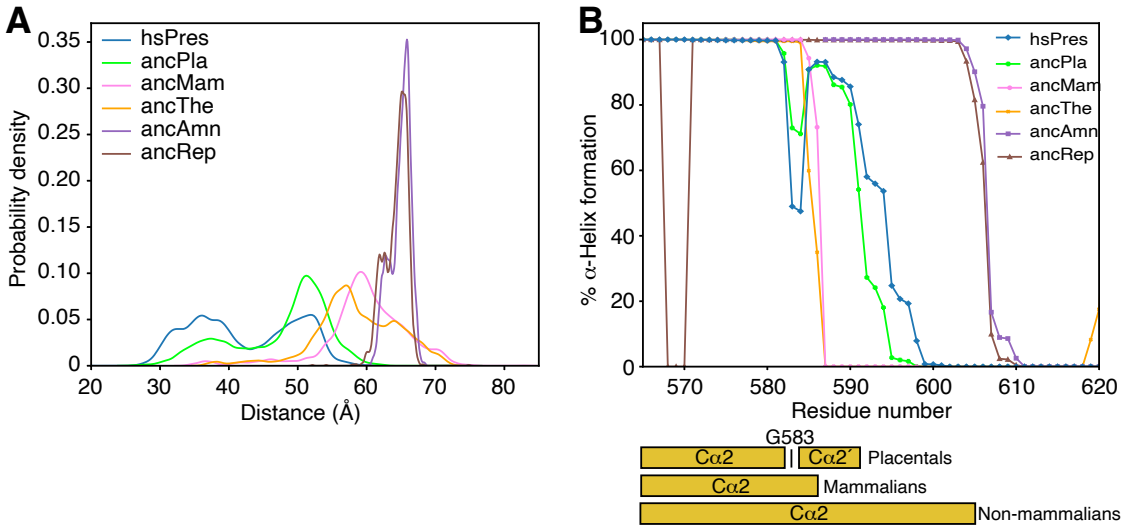

Figure 10. **Conformational and secondary structure analysis of the IVS-loop**(A) Distribution of the distance between the COM of the IVS-loop of one monomer and the chloride-binding site of the adjacent monomer obtained from the models. (B) Percentage of alpha-helix conformation for each residue in the IVS of models. The plot show the percentage of models in which each residue is assigned an alpha-helix conformation by DSSP [61]. The dark yellow blocks below the panel highlight the length of the helix for each prestin group (Placental, Mammalians and Non-mammalians) and the location of residue G583. The residue numbers correspond to hsPres.

mammals (ancPla and hsPres), show a distinct break in Cα 2, allowing the IVS-loop to adopt conformations closer to or farther from the entry of the IC (Figure 10 CD). To quantify this, we measured the distance between the center of mass (COM) of the IVS-loop and the COM of the chloride binding site of the adjacent monomer (Figure 10 F) and the helical content in the IVS of the models (Figure 10 G). Our results identified two distinct structural states in placental mammals (bimodal distribution), contrasting with earlier-mammalian and non-mammalian models that predominantly retain a single "far" conformation characterized by a continuous Cα2 helix. Our findings suggest that intermediate and late substitutions significantly altered the IVS-loop in mammalian ancestors, introducing a structural hinge near residue G583 (Figure 10 G) and a unique negatively charged patch (NP) close to the chloride entry/exit point of the adjacent monomer. Although previous studies have indicated that these charged residues slightly influence nonlinear capacitance (NLC) [35], their precise functional role remains unclear. However, the distinct conformation of the placental IVS-loop raises the possibility that it could modulate chloride ion dynamics by

restricting ion exit or trapping ions near the binding site, potentially influencing voltage sensing or allosteric coupling - an idea supported by recent findings in SLC26A9 that point in a similar direction[60].

In summary, the IVS-loop of the STAS domain stands out as a highly diverse and lineage-specific region that underwent substantial remodeling during prestin evolution. Structural and sequence changes in placental mammals, including the formation of a hinge at G583, the emergence of a negatively charged patch, and associated substitutions in neighboring helices, appear to support a unique conformation near the intracellular entrance of the adjacent protomer. Although the precise functional consequences remain to be determined, our results suggest that these changes could contribute to fine-tuning of the voltage sensitivity and chloride accessibility, highlighting the IVS-loop as a potential regulatory element in the electromechanical behavior of prestin.

A structural and evolutionary model for the emergence of area-motor function

Our findings recapitulate the progression of prestin function from ion transport in non-mammals through intermediate area-motor adaptations in monotremes to robust, finely tuned electromotility and corresponding frequency selectivity in therian mammals by a distributed remodeling of its architecture as it transitioned from a passive anion transporter to an active area-motor protein.

Although the overall scaffold of the TMD and STAS domains remained conserved, key substitutions introduced new physicochemical properties that collectively support the voltage-driven mechanical output.

In the TMD, substitutions altered membrane-facing surfaces and interhelical contacts. Aromatic and polar residues became more prevalent at the protein-lipid interface, potentially enhancing membrane anchoring and deformation.

The most striking innovations occurred in the IVS-loop. This flexible element underwent structural rearrangements in placental mammals, adopting a conformation that places a negatively charged patch near the ion access site, a feature that may directly modulate chloride access or voltage sensitivity.

Together, these changes support an evolutionary scenario in which the area-motor function

emerged through fine-tuning of existing elements within a conserved scaffold. This mosaic of adaptations may be the basis for the ability of prestin to convert voltage into mechanical work with extraordinary speed and precision.

CONCLUSIONS

Our findings provide a structural and evolutionary framework for understanding how prestin acquired its unique area-motor function in mammals. By integrating ancestral sequence reconstruction with structural modeling and comparative analysis, we reveal that the transformation of prestin from a canonical anion transporter into a voltage-sensitive motor protein involved a distributed set of molecular innovations.

Rather than arising from a single defining mutation or domain acquisition, the functional shift of prestin was driven by the accumulation of substitutions that modulate membrane embedding, helix packing, and interdomain communication. These include changes to lipid-facing residues in the transmembrane domain and reorientation of flexible loop regions.

This stepwise repurposing of conserved structural elements offers a model for how novel functional traits can evolve through subtle refinement of existing architectures, illustrating how exaptation operates at the molecular level[62]. Our work highlights the broader principles of functional innovation in membrane proteins.

METHODS

Multiple sequence alignment, phylogenetic inference, and ancestral sequence reconstruction

For the multiple sequence alignment (MSA) of chordate prestin, sequences were retrieved from the non-redundant protein database (nr) using BLASTp, with hsPres (Uniprot accession: P58743-1) as reference. Sequences exhibiting an identity greater than 98% were filtered through CD-HIT[63], while those with lengths greater than 870 and less than 570 residues were excluded. The resulting set of sequences (n = 248, see the sequence list in Supplementary Tables S6to S9) was aligned with a structural profile derived from the Cryo-EM structures of hsPres ([27]; PDB-ID: 7GLU), ttPres ([24]; PDB-ID: 7S8X) and muPres

([28];PDB-ID: 7SUN) using ClustalW[64] and STAMP[65]. Evolutive models were selected using SMS2.0[66], followed by inference of maximum likelihood (ML) phylogenetic trees using PhyML[67]. Ancestral sequences were inferred using the empirical Bayes method with PAML 4.4[68], employing the Lazarus tool as described by Handson-Smith[69]. Probability calculations for each amino acid were calculated at each alignment position for each target node, selecting the amino acids with the highest probabilities. Gap positions were inferred through machine learning (ML), using the discrete character model in Mesquite[70] as previously reported[71].

Generation of structural models

Full-length dimeric structural predictions of ancestral prestin sequences together with human prestin (hsPres), chicken (chkPres) and other representatives of mammalian and non-mammalian prestin (see Supplementary Figure S5) were generated using AlphaFold2-multimer(V3) [36, 37] within the colabfold-batch implementation 1.5.5[72]. We used five recycles and five ensembles to produce five models for each sequence. The model with the best ranking after relaxation was selected for further analysis. Templates were not used in this process.

Conformational sampling with AF2

We enhanced the conformational sampling of AlphaFold2-multimer(V3) using multiple seeds and the *dropout* option that introduces epistemic uncertainty and leads to a wider exploration of potential structures by the model[41]. We used 256 seeds with 1 recycle and 1 ensemble to generate 5 models per seed for a total of 1280 models per sequence. All models were considered for analysis.

Data analysis and visualization

The analysis of structural models was performed using VMD[73] plugins and custom Tcl and Python scripts. Distance measurements for intramonomer distances as shown as a combination of the two monomers. The intermonomer distances are shown as combinations

of distances A-B and B-A.

The assignment of a secondary structure to follow the conformations of Cα2 was done with DSSP [61]. Molecular renderings were performed with VMD.

DATA AVAILABILITY

All the outputs from ASR and AF2 structure predictions can be found at DOI:10.5281/zenodo.15197370

AUTHOR CONTRIBUTIONS

Nicolas Fuentes-Ugarte: Investigation, Formal Analysis, Visualization, Writing – Review & Editing. **Tiaren Ruiz-Rojas**: Investigation, Formal Analysis, Visualization, Writing – Review & Editing. **Alvaro Ruiz-Fernandez**: Writing – Review & Editing **Jose Antonio Garate**: Writing – Review & Editing. **Victor Castro-Fernandez**: Investigation, Conceptualization, Supervision, Writing – Original Draft Preparation, Writing – Review & Editing. **Raul Araya-Secchi**: Investigation, Conceptualization, Funding Acquisition, Writing – Original Draft Preparation, Writing – Review & Editing, Project Administration.

ACKNOWLEDGMENTS

This work is supported by the following grants: ANID FONDECYT Regular 1231164 and ANID PAI 77200112 (RAS),ANID FONDECYT Regular 1221260 (JAG), ANID FONDECYT De Iniciación 11221268 (ARF), ANID FONDECYT Regular 1221667 (VCF), ANID Beca Doctorado Nacional 21221449 (NFU) and Financiamiento Basal para Centros Cientificos y Tecnologicos de Excelencia de ANID" Centro Ciencia& Vida, FB210008 (to Fundación Ciencia & Vida). The authors thank Felipe Engelberger for his helpful advice and discussion.

CONFLICT OF INTEREST

The authors declare no conflicts of interest.

REFERENCES

[1] William E. Brownell, Charles R. Bader, Daniel Bertrand, and Yves De Ribaupierre. Evoked mechanical responses of isolated cochlear outer hair cells. *Science*, 227:194–196, 1 1985. ISSN 00368075. doi:10.1126/science.3966153. URL http://www.ncbi.nlm.nih.gov/pubmed/3966153.

[2] J. F. Ashmore. A fast motile response in guinea-pig outer hair cells: the cellular basis of the cochlear amplifier. *The Journal of Physiology*, 388:323–347, 7 1987. ISSN 14697793. doi:10.1113/jphysiol.1987.sp016617. URL https://pubmed.ncbi.nlm.nih.gov/3656195/.

[3] Peter Dallos and Bernd Fakler. Prestin, a new type of motor protein. *Nature Reviews Molecular Cell Biology*, 2002. doi:10.1038/nrm730.

[4] P. Dallos, X. Wu, M. A. Cheatham, J. Gao, J. Zheng, C. T. Anderson, S. Jia, X. Wang, W. H. Cheng, S. Sengupta, D. Z. He, and J. Zuo. Prestin-based outer hair cell motility is necessary for mammalian cochlear amplification. *Neuron*, 58(3):333–339, 2008. doi:10.1016/j.neuron.2008.02.028.

[5] Jonathan Ashmore. Cochlear outer hair cell motility. *Physiological Reviews*, 88:173–210, 1 2008. ISSN 0031-9333. doi:10.1152/physrev.00044.2006. URL http://physrev.physiology.org/cgi/doi/10.1152/physrev.00044.2006.

[6] Jing Zheng, Weixing Shen, David Z.Z. He, Kevin B. Long, Laird D. Madison, and Peter Dallos. Prestin is the motor protein of cochlear outer hair cells. *Nature*, 405:149–155, 5 2000. ISSN 00280836. doi:10.1038/35012009. URL http://www.ncbi.nlm.nih.gov/pubmed/10821263.

[7] Peter Dallos, Jing Zheng, and Mary Ann Cheatham. Prestin and the cochlear amplifier, 10 2006. ISSN 00223751.

[8] David B. Mount and Michael F. Romero. The slc26 gene family of multifunctional anion exchangers. *Pflugers Archiv European Journal of Physiology*, 447:710–721, 2 2004. ISSN 00316768. doi:10.1007/s00424-003-1090-3. URL http://www.ncbi.nlm.nih.gov/pubmed/12759755.

[9] Dominik Oliver, Dominik Oliver, David Z.Z. He, David Z.Z. He, Nikolaj Klöcker, Nikolaj Klöcker, Nikolaj Klöcker, Jost Ludwig, Jost Ludwig, Uwe Schulte, Uwe Schulte, Siegfried

Waldegger, Siegfried Waldegger, J. P. Ruppersberg, J. P. Ruppersberg, Peter Dallos, Peter Dallos, Bernd Fakler, Bernd Fakler, and Bernd Fakler. Intracellular anions as the voltage sensor of prestin, the outer hair cell motor protein. *Science*, 292(5525):2340–2343, June 2001. doi:10.1126/science.1060939.

[10] Xiaodong Tan, Jason L. Pecka, Jie Tang, Oseremen E. Okoruwa, Qian Zhang, Kirk W. Beisel, and David Z.Z. He. From zebrafish to mammal: Functional evolution of prestin, the motor protein of cochlear outer hair cells. *Journal of Neurophysiology*, 2011. doi:10.1152/jn.00234.2010.

[11] Thorsten J Schaechinger and Dominik Oliver. Nonmammalian orthologs of prestin (slc26a5) are electrogenic divalent/chloride anion exchangers. *Proceedings of the National Academy of Sciences of the United States of America*, 104:7693–8, 5 2007. ISSN 0027-8424. doi: 10.1073/pnas.0608583104. URL http://www.ncbi.nlm.nih.gov/pubmed/17442754http://www.pubmedcentral.nih.gov/articlerender.fcgi?artid=PMC1863495.

[12] Jost Ludwig, Dominik Oliver, Gerhard Frank, Nikolaj Klöcker, Anthony W. Gummer, and Bernd Fakler. Reciprocal electromechanical properties of rat prestin: The motor molecule from rat outer hair cells. *Proceedings of the National Academy of Sciences*, 2001. doi: 10.1073/pnas.071613498.

[13] Stephen J. Rossiter, Shuyi Zhang, and Yang Liu. Prestin and high frequency hearing in mammals. *Communicative Integrative Biology*, 2011. doi:10.4161/cib.4.2.14647.

[14] Lucía F. Franchini and A. Belén Elgoyhen. Adaptive evolution in mammalian proteins involved in cochlear outer hair cell electromotility. *Molecular Phylogenetics and Evolution*, 41:622–635, 12 2006. ISSN 10557903. doi:10.1016/j.ympev.2006.05.042. URL https://pubmed.ncbi.nlm.nih.gov/16854604/.

[15] Oseremen E. Okoruwa, Michael D. Weston, Divvya C. Sanjeevi, Amanda R. Millemon, Bernd Fritzsch, Richard Hallworth, and Kirk W. Beisel. Evolutionary insights into the unique electromotility motor of mammalian outer hair cells. *Evolution Development*, 2008. doi:10.1111/j.1525-142x.2008.00239.x.

[16] Liu Z, Li GH, Huang JF, Murphy RW, and Shi P. Hearing aid for vertebrates via multiple episodic adaptive events on prestin genes. *Mol Biol Evol*, 29(9):2187–98, Sep 2012. doi: 10.1093/molbev/mss087.

[17] M. Schänzler and C. Fahlke. Anion transport by the cochlear motor protein prestin. *The Journal of Physiology*, 590:259–272, 2011. doi:10.1113/jphysiol.2011.209577.

[18] P. Mistrík, N. Daudet, K. Morandell, and J. F. Ashmore. Mammalian prestin is a weak cl-/hco3 - electrogenic antiporter. *Journal of Physiology*, 590:5597–5610, 11 2012. ISSN 00223751. doi:10.1113/jphysiol.2012.241448. URL http://www.ncbi.nlm.nih.gov/pubmed/22890707http://www.pubmedcentral.nih.gov/articlerender.fcgi?artid=PMC3528980.

[19] Oseremen E. Okoruwa, Michael D. Weston, Divvya C. Sanjeevi, Amanda R. Millemon, Bernd Fritzsch, Richard Hallworth, and Kirk W. Beisel. Evolutionary insights into the unique electromotility motor of mammalian outer hair cells. *Evolution & Development*, 10:300–315, 5 2008. ISSN 1520541X. doi:10.1111/j.1525-142X.2008.00239.x. URL http://doi.wiley.com/10.1111/j.1525-142X.2008.00239.x.

[20] T. J. Schaechinger, D. Gorbunov, C. R. Halaszovich, T. Moser, S. Kügler, B. Fakler, and D. Oliver. A synthetic prestin reveals protein domains and molecular operation of outer hair cell piezoelectricity. *EMBO Journal*, 30(14):2793–2804, 2011. doi:10.1038/emboj.2011.202.

[21] Jie Tang, Jason L. Pecka, Xiaodong Tan, Kirk W. Beisel, and David Z.Z. He. Engineered pendrin protein, an anion transporter and molecular motor. *Journal of Biological Chemistry*, 286:31014–31021, 9 2011. ISSN 00219258. doi:10.1074/jbc.M111.259564. URL http://www.ncbi.nlm.nih.gov/pubmed/21757707http://www.pubmedcentral.nih.gov/articlerender.fcgi?artid=PMC3162460.

[22] Xiaodong Tan, Jason L. Pecka, Jie Tang, Sándor Lovas, Kirk W. Beisel, and David Z.Z. He. A motif of eleven amino acids is a structural adaptation that facilitates motor capability of eutherian prestin. *Journal of Cell Science*, 2012. doi:10.1242/jcs.097337.

[23] Makoto Kuwabara, Koichiro Wasano, Satoe Takahashi, Justin Bodner, Tomotaka Komori, Tomotaka Komori, Tomotaka Komori, Sotaro Uemura, Jing Zheng, Tomohiro Shima, and Kazuaki Homma. The extracellular loop of pendrin and prestin modulates their voltage-sensing property. *Journal of Biological Chemistry*, 293(26):9970–9980, June 2018. doi:10.1074/jbc.ra118.001831.

[24] Navid Bavi, Michael Clark, Gloria Contreras, Rong Shen, Bharat Reddy, Wieslawa Milewski, and Eduardo Perozo. The conformational cycle of prestin underlies outer-hair cell electromotility. *Nature*, 2021. doi:10.1038/s41586-021-04152-4.

[25] B Currall, D Rossino, H Jensen-Smith, and R Hallworth. The roles of conserved and non-conserved cysteinyl residues in the oligomerization and function of mammalian prestin. *J Neurophysiol*, 106(5):2358–67, Nov 2011. doi:10.1152/jn.00496.2011.

[26] C Izumi, JE Bird, and KH Iwasa. Membrane thickness sensitivity of prestin orthologs: the evolution of a piezoelectric protein. *Biophys J*, 100(11):2614–22, Jun 2011. doi:10.1016/j.bpj.2011.04.032.

[27] J Ge, J Elferich, S Dehghani-Ghahnaviyeh, Z Zhao, M Meadows, H von Gersdorff, E Tajkhorshid, and E Gouaux. Molecular mechanism of prestin electromotive signal amplification. *Cell*, 184(18):4669–4679.e13, 2021. ISSN 0092-8674. doi:10.1016/j.cell.2021.07.034. URL https://www.sciencedirect.com/science/article/pii/S0092867421008824. Epub 2021 Aug 13.

[28] Carmen Butan, Qiang Song, Jun-Ping Bai, Winston J T Tan, Dhasakumar Navaratnam, and Joseph Santos-Sacchi. Single particle cryo-EM structure of the outer hair cell motor protein prestin. *Nat. Commun.*, 13(1):290, January 2022.

[29] Makoto F. Kuwabara. Elevator-like movements of prestin mediate outer hair cell electromotility. *Nature Communications*, 2023. doi:10.1038/s41467-023-42489-8.

[30] Sepehr Dehghani-Ghahnaviyeh, Zhiyu Zhao, and Emad Tajkhorshid. Lipid-mediated prestin organization in outer hair cell membranes and its implications in sound amplification. *Nature Communications*, 13(1):6877, November 2022. ISSN 2041-1723. doi:10.1038/s41467-022-34596-9. URL https://doi.org/10.1038/s41467-022-34596-9.

[31] Volodymyr Rybalchenko and Joseph Santos-Sacchi. Anion control of voltage sensing by the motor protein prestin in outer hair cells. *Biophysical Journal*, 2008. doi:10.1529/biophysj.108.134197.

[32] Jun Ping Bai, Alexei Surguchev, Simone Montoya, Peter S. Aronson, Joseph Santos-Sacchi, and Dhasakumar Navaratnam. Prestin's anion transport and voltage-sensing capabilities are independent. *Biophysical Journal*, 96:3179–3186, 4 2009. ISSN 15420086. doi:10.1016/j.bpj.2008.12.3948. URL http://www.ncbi.nlm.nih.gov/pubmed/19383462http://www.pubmedcentral.nih.gov/articlerender.fcgi?artid=PMC2718310.

[33] Lei Song, Lei Song, Joseph Santos-Sacchi, and Joseph Santos-Sacchi. Disparities in voltage-sensor charge and electromotility imply slow chloride-driven state transitions in the solute carrier SLC26a5. *Proceedings of the National Academy of Sciences of the United States of*

America, 110(10):3883–3888, March 2013. doi:10.1073/pnas.1218341110.

[34] Dmitry Gorbunov, Mattia Sturlese, Florian Nies, Murielle Kluge, Massimo Bellanda, Roberto Battistutta, and Dominik Oliver. Molecular architecture and the structural basis for anion interaction in prestin and SLC26 transporters. *Nature Communications*, 5(1):3622–3622, April 2014. doi:10.1038/ncomms4622.

[35] J. P. Bai, D. Navaratnam, H. Samaranayake, and J. Santos-Sacchi. En block c-terminal charge cluster reversals in prestin (slc26a5): effects on voltage-dependent electromechanical activity. *Neuroscience Letters*, 404(3):270–275, Sep 2006. doi:10.1016/j.neulet.2006.05.062.

[36] J. Jumper et al. Highly accurate protein structure prediction with alphafold. *Nature*, 596: 583–589, Aug 2021.

[37] R. Evans et al. Protein complex prediction with alphafold-multimer. *bioRxiv*, 2021. doi: 10.1101/2021.10.04.463034v1. Preprint.

[38] S.E. Evans. Evolution and phylogeny of amniotes. In M.D. Binder, N. Hirokawa, and U. Windhorst, editors, *Encyclopedia of Neuroscience*. Springer, Berlin, Heidelberg, 2009. doi: 10.1007/978-3-540-29678-2_3113.

[39] A. Meyer and R. Zardoya. Recent advances in the (molecular) phylogeny of vertebrates. *Annual Review of Ecology, Evolution, and Systematics*, 34(1):311–338, 2003.

[40] GKA Hochberg and JW Thornton. Reconstructing ancient proteins to understand the causes of structure and function. *Annual Review of Biophysics*, 46:247–269, 2017. doi: 10.1146/annurev-biophys-070816-033631.

[41] Björn Wallner. AFsample: improving multimer prediction with AlphaFold using massive sampling. *Bioinformatics*, 39(9):btad573, 09 2023. ISSN 1367-4811. doi:10.1093/bioinformatics/btad573. URL https://doi.org/10.1093/bioinformatics/btad573.

[42] Xiaodong Tan, Jason L. Pecka, Jie Tang, Oseremen E. Okoruwa, Qian Zhang, Kirk W. Beisel, and David Z.Z. He. From Zebrafish to Mammal: Functional Evolution of Prestin, the Motor Protein of Cochlear Outer Hair Cells. *Journal of Neurophysiology*, 105(1):36–44, January 2011. doi:10.1152/jn.00234.2010.

[43] David Z.Z. He, Sándor Lovas, Yu Ai, Yi Li, and Kirk W. Beisel. Prestin at year 14: Progress and prospect. *Hearing Research*, 311:25–35, May 2014. doi:10.1016/j.heares.2013.12.002.

[44] K.H. Iwasa. Effect of stress on the membrane capacitance of the auditory outer hair cell. *Biophysical Journal*, 65(1):492–498, 1993. ISSN 0006-3495. doi: https://doi.org/10.1016/S0006-3495(93)81053-1. URL https://www.sciencedirect.com/science/article/pii/S0006349593810531.

[45] Joseph Santos-Sacchi, Weixing Shen, Jing Zheng, and Peter Dallos. Effects of membrane potential and tension on prestin, the outer hair cell lateral membrane motor protein. *The Journal of Physiology*, 531(3):661–666, 2001. doi:https://doi.org/10.1111/j.1469-7793.2001.0661h.x. URL https://physoc.onlinelibrary.wiley.com/doi/abs/10.1111/j.1469-7793.2001.0661h.x.

[46] Joseph Santos-Sacchi and Winston Tan. Complex nonlinear capacitance in outer hair cell macro-patches: effects of membrane tension. *Scientific Reports*, 10(1), 2020. doi: 10.1038/s41598-020-63201-6. URL https://www.scopus.com/inward/record.uri?eid=2-s2.0-85083235474&doi=10.1038%2fs41598-020-63201-6&partnerID=40&md5=ea8b7e9d127c64a13724d45c1b6ed492.

[47] Jing Fang, Chisako Izumi, and Kuni H. Iwasa. Sensitivity of prestin-based membrane motor to membrane thickness. *Biophysical Journal*, 98(12):2831–2838, 2010. doi: 10.1016/j.bpj.2010.03.034.

[48] Chisako Izumi, Jonathan E. Bird, and Kuni H. Iwasa. Membrane thickness sensitivity of prestin orthologs: The evolution of a piezoelectric protein. *Biophysical Journal*, 2011. doi: 10.1016/j.bpj.2011.04.032.

[49] R. I. Kamar, L. E. Organ-Darling, and R. M. Raphael. Membrane cholesterol strongly influences confined diffusion of prestin. *Biophysical Journal*, 103:1627–1636, 10 2012. ISSN 00063495. doi:10.1016/j.bpj.2012.07.052. URL http://dx.doi.org/10.1016/j.bpj.2012.07.052https://pubmed.ncbi.nlm.nih.gov/23083705/.

[50] Lavanya Rajagopalan, Jennifer N. Greeson, Anping Xia, Haiying Liu, Angela Sturm, Robert M. Raphael, Amy L. Davidson, John S. Oghalai, Fred A. Pereira, and William E. Brownell. Tuning of the outer hair cell motor by membrane cholesterol. *Journal of Biological Chemistry*, 282:36659–36670, 12 2007. ISSN 00219258. doi:10.1074/jbc.M705078200. URL http://www.jbc.org.

[51] John Sfondouris, Lavanya Rajagopalan, Fred A. Pereira, and William E. Brownell. Membrane composition modulates prestin-associated charge movement*. *Journal of Biological Chemistry*,

283(33):22473–22481, 2008. ISSN 0021-9258. doi:https://doi.org/10.1074/jbc.M803722200. URL https://www.sciencedirect.com/science/article/pii/S0021925820747794.

[52] Esther S. Brielle and Isaiah T. Arkin. Quantitative analysis of multiplex h-bonds. *Journal of the American Chemical Society*, 2020. doi:10.1021/jacs.0c04357.

[53] Kelsey A. Sparks, Nicholas J. Gleason, Renetra Gist, Rebekah Langston, Denise V. Greathouse, and Roger E. II Koeppe. Comparisons of interfacial phe, tyr, and trp residues as determinants of orientation and dynamics for gwalp transmembrane peptides. *Biochemistry*, 53 (22):3637–3645, 2014. doi:10.1021/bi500439x. URL https://doi.org/10.1021/bi500439x. PMID: 24829070.

[54] Coral del Val, Stephen H. White, and Ana-Nicoleta Bondar. Ser/thr motifs in transmembrane proteins: Conservation patterns and effects on local protein structure and dynamics. *The Journal of Membrane Biology*, 245(11):717–730, 2012. doi:10.1007/s00232-012-9452-4. URL https://doi.org/10.1007/s00232-012-9452-4.

[55] Shyam S. Krishnakumar and Erwin London. The control of transmembrane helix transverse position in membranes by hydrophilic residues. *Journal of Molecular Biology*, 374 (5):1251–1269, 2007. ISSN 0022-2836. doi:https://doi.org/10.1016/j.jmb.2007.10.032. URL https://www.sciencedirect.com/science/article/pii/S0022283607013708.

[56] Jacob P. Keller, Kazuaki Homma, Chongwen Duan, Jing Zheng, Mary Ann Cheatham, and Peter Dallos. Functional regulation of the slc26-family protein prestin by calcium/calmodulin. *Journal of Neuroscience*, 2014. doi:10.1523/jneurosci.4020-13.2014.

[57] Satoe Takahashi and Kazuaki Homma. The molecular principles underlying diverse functions of the SLC26 family of proteins. *J. Biol. Chem.*, 300(5):107261, May 2024.

[58] Kazuaki Homma, Kazuaki Homma, Katharine Miller, Katharine K. Miller, Charles T. Anderson, Charles T. Anderson, Charles T. Anderson, Charles T. Anderson, Soma Sengupta, Soma Sengupta, Guo Guang Du, Guo Guang Du, Salvador Aguiñaga, Salvador Aguinaga, Mary Ann Cheatham, Mary Ann Cheatham, Peter Dallos, Peter Dallos, Jing Zheng, and Jing Zheng. Interaction between cftr and prestin (slc26a5). *Biochimica et Biophysica Acta*, 2010. doi:10.1016/j.bbamem.2010.02.001.

[59] Carol A. Bertrand, Shalini Mitra, Sanjay Mishra, Xiaohui Wang, Yu Zhao, Joseph M. Pilewski, Dean R. Madden, and Raymond A. Frizzell. The cftr trafficking mutation f508del inhibits the constitutive activity of slc26a9. *Ajp Lung Cellular and Molecular Physiology*, 2017. doi:

10.1152/ajplung.00178.2016.

[60] An-Ping Chen, Heather Holmes, James W. Decker, Min-Hwang Chang, and Michael F. Romero. Disorder within order: identification of the disordered loop of stas domain as the inhibitory domain in slc26a9 chloride channel. *Journal of Biological Chemistry*, page 108145, 2024. ISSN 0021-9258. doi:https://doi.org/10.1016/j.jbc.2024.108145. URL https://www.sciencedirect.com/science/article/pii/S0021925824026474.

[61] Wolfgang Kabsch and Christian Sander. Dictionary of protein secondary structure: Pattern recognition of hydrogen-bonded and geometrical features. *Biopolymers*, 22(12):2577–2637, 1983. doi:https://doi.org/10.1002/bip.360221211. URL https://onlinelibrary.wiley.com/doi/abs/10.1002/bip.360221211.

[62] Jürgen Brosius. Exaptation at the molecular genetic level. *Science China Life Sciences*, 62 (4):437–452, 2019. doi:10.1007/s11427-018-9447-8.

[63] Y. Huang, B. Niu, Y. Gao, L. Fu, and W. Li. Cd-hit suite: A web server for clustering and comparing biological sequences. *Bioinformatics*, 26(5):680–682, 2010. doi: 10.1093/bioinformatics/btq003.

[64] J. D. Thompson, D. G. Higgins, and T. J. Gibson. Clustal w: Improving the sensitivity of progressive multiple sequence alignment through sequence weighting, position-specific gap penalties and weight matrix choice. *Nucleic Acids Research*, 22(22):4673–4680, 1994. doi: 10.1093/nar/22.22.4673.

[65] R. B. Russell and G. J. Barton. Multiple protein sequence alignment from tertiary structure comparison: Assignment of global and residue confidence levels. *Proteins: Structure, Function, and Bioinformatics*, 14(2):309–323, 1992. doi:10.1002/prot.340140216.

[66] V. Lefort, J. E. Longueville, and O. Gascuel. Sms: Smart model selection in phyml. *Molecular Biology and Evolution*, 34(9):2422–2424, 2017. doi:10.1093/MOLBEV/MSX149.

[67] S. Guindon, J. F. Dufayard, V. Lefort, M. Anisimova, W. Hordijk, and O. Gascuel. New algorithms and methods to estimate maximum-likelihood phylogenies: Assessing the performance of phyml 3.0. *Systematic Biology*, 59(3):307–321, 2010. doi:10.1093/sysbio/syq010.

[68] Z. Yang. Paml 4: Phylogenetic analysis by maximum likelihood. *Molecular Biology and Evolution*, 24(8):1586–1591, 2007. doi:10.1093/molbev/msm088.

[69] V. Hanson-Smith, B. Kolaczkowski, and J. W. Thornton. Robustness of ancestral sequence reconstruction to phylogenetic uncertainty. *Molecular Biology and Evolution*, 27(9):1988–1999,

2010. doi:10.1093/molbev/msq081.

[70] W. P. Maddison and D. R. Maddison. Mesquite: a modular system for evolutionary analysis. Version 3.81, 2023. URL http://www.mesquiteproject.org.

[71] Victor Castro-Fernandez, Ariel Herrera-Morande, Rodrigo Zamora, Fernando Merino, Felipe Gonzalez-Ordenes, Fernando Padilla-Salinas, Herika M. Pereira, José Brandão-Neto, Richard C. Garratt, and Victor Guixe. Reconstructed ancestral enzymes reveal that negative selection drove the evolution of substrate specificity in adp-dependent kinases. *Journal of Biological Chemistry*, 292(38):15598–15610, Sep 2017. doi:10.1074/jbc.M117.790865. Erratum in: J Biol Chem. 2017 Dec 22;292(51):21218.

[72] M. Mirdita et al. Colabfold: making protein folding accessible to all. *Nature Methods*, 19: 679–682, May 2022.

[73] William Humphrey, Andrew Dalke, and Klaus Schulten. VMD – Visual Molecular Dynamics. *Journal of Molecular Graphics*, 14:33–38, 1996. doi:10.1016/0263-7855(96)00018-5.

[74] Justin D. Walter, Justin D. Walter, Marta Sawicka, Marta Sawicka, Raimund Dutzler, and Raimund Dutzler. Cryo-EM structures and functional characterization of murine Slc26a9 reveal mechanism of uncoupled chloride transport. *eLife*, 8, July 2019. doi:10.7554/elife.46986.

[75] Sudhir Kumar, Michael Suleski, Jack M Craig, Adrienne E Kasprowicz, Maxwell Sanderford, Michael Li, Glen Stecher, and S Blair Hedges. Timetree 5: An expanded resource for species divergence times. *Molecular Biology and Evolution*, 39(8):msac174, 08 2022. ISSN 1537-1719. doi:10.1093/molbev/msac174. URL https://doi.org/10.1093/molbev/msac174.